

A size-dependent study on buckling and post-buckling behavior of imperfect piezo-flexomagnetic nano-plate strips

Hamed Momeni-Khabisi^a and Masoud Tahani*

Department of Mechanical Engineering, Ferdowsi University of Mashhad, Mashhad, Iran

(Received December 24, 2021, Revised February 1, 2022, Accepted February 2, 2022)

Abstract. In the present study, the nonlocal strain gradient theory is used to predict the size-dependent buckling and post-buckling behavior of geometrically imperfect nano-scale piezo-flexomagnetic plate strips in two modes of direct and converse flexomagnetic effects. The first-order shear deformation plate theory is used to analyze analytically nano-strips with simply supported boundary conditions. The nonlinear governing equations of equilibrium and associated boundary conditions are derived using the principle of minimum total potential energy with consideration of the von Kármán-type of geometric non-linearity. A closed-form solution of governing differential equation is obtained, which is easily usable for engineers and designers. To validate the presented formulations, whenever possible, a comparison with the results found in the open literature is reported for buckling loads. A parametric study is presented to examine the effect of scaling parameters, plate slenderness ratio, temperature, the mid-plane initial rise, flexomagnetic coefficient, different temperature distributions, and magnetic potential, in case of the converse flexomagnetic effect, on buckling and post-buckling loads in detail.

Keywords: flexomagnetic; geometrical imperfection; nano-plate strip; nonlocal strain gradient theory; piezomagnetic; post-buckling

1. Introduction

Advances in nanotechnology and the increase in the use of nano-scale structures in applications such as measuring equipment and medicine have led to extensive research into micro- and nano-electromechanical systems (MEMs/NEMs). These systems have many applications in various industries such as aerospace, robotic, electronic, and military. Attention to the flexo effect in the industry has increased rapidly because it is not restricted to the crystalline structure of materials, unlike the piezo effect which is restricted by the crystal symmetries. This indicates the potential for the development of piezomagnetic-like structures without the use of any conventional piezomagnetic (PM) materials. Like the important applications of the PM effect on nano-motors, nano-memories, nano-sensors, nano-actuators, and energy harvesters, in the future, the flexomagnetic effect may also play such an important role in the construction of these small-scale devices. They can be utilized as nano-sensors to measure magnetic potentials/mechanical deflections or as nano-actuators to apply magnetic loads in such devices (Bagheri and Tadi Beni 2021, Eliseev *et al.* 2009, 2019, Fahrner 2005, Lee *et al.* 2011, Lukashev and Sabirianov 2010, Moosavi *et al.* 2017, Shingare and Kundalwal (2019).

Post-buckling analysis of nanostructures with and without geometrical imperfection is of interest to researchers

(e.g., Asrari *et al.* 2020, Barati and Zenkour 2019, Reddy 2010, Mohamed *et al.* 2019). At nano-scales the effect of size is more important in buckling analysis. Because of discontinuity in the structures at nano-scale, the size-dependent theories are employed to develop an equivalent continuum model for these nanostructures. Indeed, in continuum theories, the space between the atoms compared to the main dimensions of the structure is ignored. One of the best and most widely used theories to take into account the size-dependency at micro/nano scales is the nonlocal strain gradient (NSG) theory proposed by Lim *et al.* (2015). This model couples Eringen's nonlocal theory and strain gradient theory of Mindlin. The NSG theory has been incorporated in a lot of research in the field of nanostructures (e.g., Fenjan *et al.* 2020, Mir and Tahani 2020, Radgolchin and Tahani 2021).

The piezomagnetic/piezoelectric effect is the coupling between uniform mechanical strain and magnetic/electric potential. The coupling between non-uniform mechanical strain and the induced magnetic/electric field is defined as the flexomagnetic/flexoelectric effect. The flexo effect is negligible at the macro-scales, but at micro/nano structures, it gains significance and becomes dominant (Eliseev *et al.* 2009, 2019, Kundalwal *et al.* 2019, Lukashev and Sabirianov 2010).

Indeed, for centrosymmetric crystals that have no PM properties, the FM properties provide the magneto-elastic coupling. The direct flexomagnetic (DFM) effect is referred to the induced magnetic polarization due to the non-uniform mechanical strain, and the converse flexomagnetic (CFM) effect is the generation of non-uniform strain in the presence of the magnetic field (Sidhardh and Ray 2018, Zhang *et al.* 2019).

*Corresponding author, Professor,
E-mail: mtahani@um.ac.ir

^aPh.D. Student,
E-mail: hamedmomeni-khabisi@mail.um.ac.ir

Although a lot of research has been done in piezo effect (e.g., Kundalwal and Ray 2016, Mirjavadi *et al.* 2019, Moradi *et al.* 2020, Sun *et al.* 2017), there is little research on the FM effect and this field is still in its infancy. Some research works presented experimental evidence supporting the FM effect. For example, Belyaev *et al.* (2020) experimentally studied the flexomagnetic effect in nanocrystalline thin permalloy film. They induced the strain gradient in the film and observed the unidirectional magnetic anisotropy that can be explained by the FM effect. The value of the FM coefficient was obtained $1.5 \times 10^{-3} \text{ Tm}$ for the $\text{Ni}_{71.5}\text{Fe}_{28.5}$ wt.% film that shows the significant role of the FM effect. Zhang *et al.* (2012) proposed that the flexoelectric and flexomagnetic effects may be responsible for the giant piezoelectricity and the enhanced magnetism across the phase boundaries of BiFeO_3 films. Also, based on measurements of atomic force microscopy and transmission electron microscopy they indicated that the role of the phase boundaries in the enhanced piezoelectricity is crucial.

Eliseev *et al.* (2009) investigated the spontaneous flexoeffect on the nanoferroics. In case of nanorods and thin pills, they found an exact solution for the spatially inhomogeneous mechanical displacement vector. As they discussed, the flexoeffect is the reason for the symmetry changes that lead to the phase-transition temperature change and the nanoparticle shape distortions. Pyatakov and Zvezdin (2009) studied dynamic behavior of magnon spectra due to inhomogeneous magnetoelectric interaction. In their research, they found a relationship between the flexo-magnetoelectric interaction and the effect of ferroelectric domain structure on antiferromagnetic structure. Lukashov and Sabirianov (2010) investigated the DFM effect in Mn_3GaN , and they found a linear dependency between the magnetization and the flexure. They estimated the flexomagnetic coefficient and compared the contribution of the FM effect to the induced magnetization with the case of nonlinear effect. In bulk and nano-scale materials, Eliseev *et al.* (2011) showed that the flexomagnetic effect leads to a new linear flexo-magnetoelectric coupling. Also, they demonstrated the proportionality between the linear flexo-magnetoelectric coupling and the product of the gradients of (anti) magnetization, polarization, flexomagnetic, and flexoelectric tensors. They found that the improper ferroelectricity in both bulk and nano-scale (anti) ferromagnetics may be due to the FM effect. Using the symmetry theory, they showed that the FM effect strongly increases the number of the magnetoelectric multiferroic materials. Shi *et al.* (2019) proposed a way to enhance the functionality of devices at the nano-scale. Their investigation on VSe_2 monolayers showed that structural wrinkling or corrugation causes a large strain gradient and induces the flexomagnetic and flexoelectric effects simultaneously.

Sidhardh and Ray (2018) using the variational principle and the strain gradient theory of elasticity, derived the general tensorial form of the governing differential equations and corresponding end conditions for the linear bending analysis of a cantilever piezo-flexomagnetic (PFM)

Euler-Bernoulli nanobeam. They solved these equations for both direct and converse FM effects, and presented the analytical expressions for the ME response. They showed that the FM effect is more important at low dimensions. Zhang *et al.* (2019) investigated the linear static bending of piezomagnetic Euler-Bernoulli nanobeam based on the strain gradient theory considering the flexomagneticity and surface effects. They used the Hamilton principle to derive the governing equations and associated boundary conditions. They presented the analytical expressions for DFM and CFM effects for different boundary conditions and demonstrated that the flexomagnetic effect is dependent on size. Malikan *et al.* (2020) using the nonlocal strain gradient theory of elasticity, analyzed the post-buckling of piezo-flexomagnetic nanobeams with various boundary conditions. They used the Euler-Bernoulli beam theory and von-Kármán strains in a closed-circuit state (converse FM) to derive a mathematical model. From their results, one can find that the FM effect in nanobeams with lower degrees of freedom in the boundary conditions is more pronounced. Furthermore, Malikan and Eremeyev (2021a) presented the effect of converse flexomagneticity on the biaxial buckling of a piezomagnetic nano-plate. Using the classical plate theory, infinitesimal strains, NSG theory, and with the application of Hamilton's principle, the governing equations of equilibrium were derived and then solved for simply supported and clamped boundary conditions. Another research on piezo-flexomagnetic nanostructures was performed by Shi *et al.* (2021) in which they studied the piezo-flexoelectric and piezo-flexomagnetic effects to analyze nanocomposites. The governing differential equations and related boundary conditions in the tensorial form were derived. As an example, they investigated the magnetoelectric response of bilayer cantilever nanobeams, considering the piezoeffect and flexoeffect with the application of classical theory and a closed-form expression for magnetoelectric voltage was presented. Sladek *et al.* (2021) investigated the direct FM effect on a cantilever nanobeam considering the Timoshenko beam theory with linear strains. One of their noteworthy achievements was reducing the rotations and transverse deflections due to the FM effect. Malikan and Eremeyev (2021b) reported an investigation on the influence of the flexomagnetic effect in a shear deformable piezomagnetic nanostructure. The Timoshenko beam model with converse flexomagnetic effect and linear strains was used, and the effect of size was implemented by the NSG theory. After derivation of the governing differential equations of equilibrium, the Galerkin weighted residual method was used to evaluate the critical buckling load in case of the simply supported end conditions. Cai *et al.* (2020) by relying on finite element simulation and experimental approach, showed that very large strain gradients can be obtained at moderate temperatures, causing the effects of flexomagnetic and flexoelectric.

Based on the reviewed paper, the buckling and post-buckling analysis of piezo-flexomagnetic nano-plate strips have not been done yet. Furthermore, both direct and converse flexomagnetic effects, thermal environment and, the geometrical imperfection are considered simultaneously.

To derive the nonlinear size-dependent governing equations, von-Kármán strains, NSG theory and, the principle of minimum total potential energy are used. It is assumed that the nano-plate strip is simply supported at the ends. A closed-form solution is presented, and the effect of several parameters such as temperature, nonlocal and strain gradient parameters, plate slenderness ratio, the mid-plane initial rise, flexomagnetic coefficient, different temperature distributions, and magnetic potential on buckling and post-buckling loads is studied.

2. Mathematical formulation

2.1 Preliminaries

The free energy density of a PFM structure can be expressed as follows (Sidhardh and Ray (2018)):

$$U = U(\varepsilon, \eta, H) = -\frac{1}{2} \mathbf{H} \cdot \mathbf{a} \cdot \mathbf{H} + \frac{1}{2} \boldsymbol{\varepsilon} : \mathbf{C} : \boldsymbol{\varepsilon} + \frac{1}{2} \boldsymbol{\eta} : \mathbf{g} : \boldsymbol{\eta} + \boldsymbol{\varepsilon} : \mathbf{r} : \boldsymbol{\eta} - \mathbf{H} \cdot \mathbf{d} : \boldsymbol{\varepsilon} - \mathbf{H} \cdot \mathbf{f} : \boldsymbol{\eta} \quad (1)$$

where $\boldsymbol{\varepsilon}$ is the strain tensor (second-order), $\boldsymbol{\eta}$ is the strain gradient tensor (third-order), \mathbf{H} is the magnetic field vector, \mathbf{a} is the magnetic permeability tensor (second-order), \mathbf{d} is the piezomagnetic tensor (third-order), \mathbf{f} is the flexomagnetic tensor (fourth-order), \mathbf{C} is the elasticity coefficient tensor (fourth-order), \mathbf{r} is the coupling tensor between the strain and strain gradient tensors (fifth-order), and \mathbf{g} is the strain gradient elasticity tensor (sixth-order).

The Green-Lagrange strain tensor and the strain gradient tensor in terms of the displacement vector are presented as:

$$\boldsymbol{\varepsilon} = \frac{1}{2} [\nabla \mathbf{u} + (\nabla \mathbf{u})^T + \nabla \mathbf{u} \cdot (\nabla \mathbf{u})^T], \quad \boldsymbol{\eta} = \nabla \boldsymbol{\varepsilon} \quad (2)$$

The relation between the magnetic field vector and the scalar magnetic potential is expressed as:

$$\mathbf{H} = -\nabla \psi \quad (3)$$

With consideration of the variables $\boldsymbol{\varepsilon}$, $\boldsymbol{\eta}$, and \mathbf{H} , the constitutive equations can be written as (Sidhardh and Ray 2018):

$$\begin{aligned} \boldsymbol{\sigma} &= \frac{\partial U}{\partial \boldsymbol{\varepsilon}} = \mathbf{C} : \boldsymbol{\varepsilon} + \mathbf{r} : \boldsymbol{\eta} - \mathbf{H} \cdot \mathbf{d} \\ \boldsymbol{\tau} &= \frac{\partial U}{\partial \boldsymbol{\eta}} = \mathbf{g} : \boldsymbol{\eta} + \boldsymbol{\varepsilon} : \mathbf{r} - \mathbf{H} \cdot \mathbf{f} \\ \mathbf{B} &= -\frac{\partial U}{\partial \mathbf{H}} = \mathbf{a} \cdot \mathbf{H} + \mathbf{d} : \boldsymbol{\varepsilon} + \mathbf{f} : \boldsymbol{\eta} \end{aligned} \quad (4)$$

where $\boldsymbol{\sigma}$ is the Cauchy-stress tensor (second-order), $\boldsymbol{\tau}$ is the higher-order stress tensor (third-order), and \mathbf{B} is the magnetic induction (or flux) vector.

2.2 Variational formulation

The principle of minimum total potential energy is defined as:

$$\delta \Pi = 0 \quad (5)$$

where $\Pi = U + V$ is called the total potential energy of the elastic body, and

$$\delta V = -\delta W_E = -\int_{\Omega} \mathbf{f} \cdot \delta \mathbf{u} \, dv - \int_{\Gamma} \mathbf{t} \cdot \delta \mathbf{u} \, ds \quad (6)$$

$$\delta U = \int_{\Omega} (\boldsymbol{\sigma} : \delta \boldsymbol{\varepsilon} + \boldsymbol{\tau} : \delta \boldsymbol{\eta} - \mathbf{B} \cdot \delta \mathbf{H}) \, dv \quad (7)$$

where W_E is the work done by external forces in a body Ω . Using the principle of minimum total potential energy, one can get the following governing equations:

$$\delta \mathbf{u} : \nabla \cdot (\boldsymbol{\sigma} - \nabla \cdot \boldsymbol{\tau}) = -\mathbf{f} \quad (8)$$

$$\delta \psi : \nabla \cdot \mathbf{B} = 0 \quad (9)$$

and related boundary conditions:

$$\delta \mathbf{u} = 0 \quad \text{or} \quad \mathbf{n} \cdot (\boldsymbol{\sigma} - \nabla \cdot \boldsymbol{\tau}) = \mathbf{t} \quad \text{on} \quad \Gamma_1 \quad (10)$$

$$\delta \psi = 0 \quad \text{or} \quad \mathbf{n} \cdot \mathbf{B} = 0 \quad \text{on} \quad \Gamma_2 \quad (11)$$

where Γ_1 denotes the portion of the boundary on which stresses or displacements are specified and Γ_2 denotes the portion of the boundary on which magnetic potential or magnetic induction are specified.

2.3 Modeling of PFM nano-plate strip in thermal environment

For a rectangular plate in the x - y plane, when the dimension along the y -axis (i.e., width b) is very long compared to the dimension along the x -axis (i.e., length a), it is treated as a plate strip. Fig. 1 shows a schematic of the problem. It is worth mentioning that two cases of rectangular plates can be treated as one-dimensional problems: beams and cylindrical bending of plate strips. When the width b (i.e., length along the y -axis) of a plate is very small compared to the length a along the x -axis, it is treated as a beam. In cylindrical bending, the plate is assumed to be a plate strip that is very long along the y -axis and has a finite dimension a along the x -axis. (Reddy 2006).

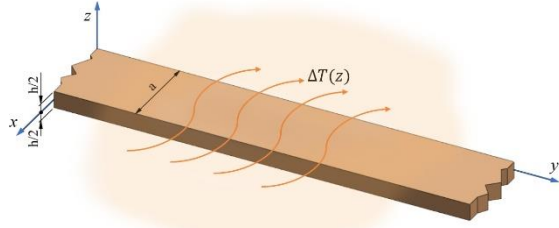
The displacement components according to the FSDP theory are given by:

$$\begin{aligned} u(x, z) &= u_0(x) + z\phi(x) \\ w(x, z) &= w_0(x) \end{aligned} \quad (12)$$

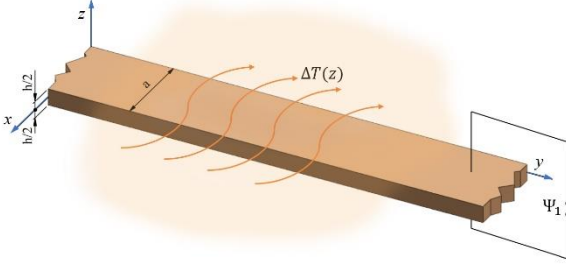
Based on the von-Kármán nonlinear strains we obtained:

$$\begin{aligned} \varepsilon_{xx} &= \varepsilon_{xx}^0 + z\varepsilon_{xx}^1 \\ \gamma_{xz} &= \gamma_{xz}^0 \\ \varepsilon_{yy} &= \varepsilon_{zz} = \gamma_{xy} = \gamma_{yz} = 0 \\ \eta_{xxz} &= \frac{d\phi}{dx} \\ \eta_{yyz} &= \eta_{xyz} = 0 \end{aligned} \quad (13)$$

where



(a) Direct flexomagnetic effect



(b) Converse flexomagnetic effect

Fig. 1 Schematic of a piezo-flexomagnetic nano-plate strip

$$\begin{aligned}\varepsilon_{xx}^0 &= \frac{du_0}{dx} + \frac{1}{2} \left(\frac{dw_0}{dx} \right)^2 \\ \gamma_{xz}^0 &= \phi + \frac{dw_0}{dx} \\ \varepsilon_{xx}^1 &= \frac{d\phi}{dx}\end{aligned}\quad (14)$$

From Eq. (4) one can write (Reddy 2006, Shi *et al.* 2021, Sidhardh and Ray 2018, Wang and Li 2021):

$$\begin{aligned}\sigma_{xx} &= Q_{11}(\varepsilon_{xx} - \alpha\Delta T) + Q_{12}(\varepsilon_{yy} - \alpha\Delta T) - d_{31}H_z \\ \sigma_{xz} &= C_{55}\gamma_{xz} \\ \tau_{xxz} &= g_{113113}\eta_{xxz} - f_{14}H_z \\ B_z &= a_{33}H_z + d_{31}\varepsilon_{xx} + f_{14}\eta_{xxz}\end{aligned}\quad (15)$$

where Q_{ij} are the plane-stress reduced stiffness coefficients and are given in Appendix A.

The simplified form of Eq. (7) with combination of Eq. (15) can be written as:

$$\delta U = \int_A \int_{-h/2}^{h/2} \left(\sigma_{xx} \delta \varepsilon_{xx} + \sigma_{xz} \delta \gamma_{xz} \right) dz dA \quad (16)$$

By substituting Eqs. (3), (13), and (14) into Eq. (16) and using the divergence theorem, one can write:

$$\begin{aligned}\delta U &= -\int_A \frac{dN_{xx}}{dx} \delta u_0 dA - \int_A \frac{d}{dx} \left(N_{xx} \frac{dw_0}{dx} \right) \delta w_0 dA - \int_A \frac{dM_{xx}}{dx} \delta \phi dA \\ &+ \int_A Q_x \delta \phi dA - \int_A \frac{dQ_x}{dx} \delta w_0 dA - \int_A \frac{dN_{xxz}}{dx} \delta \phi dA - \int_A \int_{-h/2}^{h/2} \frac{\partial B_z}{\partial z} \delta \psi dz dA \\ &+ \left[\int_0^b N_{xx} \delta u_0 dy \right]_{x=0}^{x=a} + \left[\int_0^b N_{xx} \frac{dw_0}{dx} \delta w_0 dy \right]_{x=0}^{x=a} + \left[\int_0^b M_{xx} \delta \phi dy \right]_{x=0}^{x=a} \\ &+ \left[\int_0^b Q_x \delta w_0 dy \right]_{x=0}^{x=a} + \left[\int_0^b N_{xxz} \delta \phi dy \right]_{x=0}^{x=a} + \left[\int_A B_z \delta \psi dA \right]_{z=-h/2}^{z=h/2}\end{aligned}\quad (17)$$

Note that only the z-component of the magnetic field is considered in this study. Finally, by applying the principle of minimum total potential energy, the mechanical and magnetic differential equations are obtained as:

$$\delta u_0: \quad \frac{dN_{xx}}{dx} = 0 \quad (18)$$

$$\delta w_0: \quad \frac{d}{dx} \left(N_{xx} \frac{dw_0}{dx} \right) + \frac{dQ_x}{dx} = 0 \quad (19)$$

$$\delta \phi: \quad \frac{dM_{xx}}{dx} + \frac{dN_{xxz}}{dx} - Q_x = 0 \quad (20)$$

$$\delta \psi: \quad \frac{\partial B_z}{\partial z} = 0 \quad (21)$$

The boundary conditions involve the specification of

$$\begin{aligned}\delta u_0 &= 0 \quad \text{or} \quad N_{xx} = 0 \quad \text{at} \quad x = 0, a \\ \delta w_0 &= 0 \quad \text{or} \quad N_{xx} \frac{dw_0}{dx} + Q_x = 0 \quad \text{at} \quad x = 0, a \\ \delta \phi &= 0 \quad \text{or} \quad M_{xx} + N_{xxz} = 0 \quad \text{at} \quad x = 0, a \\ \psi &= \Psi_1 \quad \text{or} \quad B_z = 0 \quad \text{at} \quad x = \pm \frac{h}{2}\end{aligned}\quad (22)$$

where the stress resultants are defined as:

$$(N_{xx}, M_{xx}) = \int_{-h/2}^{h/2} \sigma_{xx}(1, z) dz \quad (23)$$

$$Q_x = K_s \int_{-h/2}^{h/2} \sigma_{xz} dz, \quad N_{xxz} = \int_{-h/2}^{h/2} \tau_{xxz} dz$$

with $K_s = 5/6$ is the shear correction factor (Reddy 2006).

2.4 Direct flexomagnetic effect

Using Eq. (21) and the boundary condition of the magnetic induction vector, we conclude that:

$$B_z = 0 \quad \text{throughout} \quad \Omega \quad (24)$$

The magnetic potential and the z-component of the magnetic field are determined by using Eqs. (3), (13), (14), (15), and (24) as follows:

$$\begin{aligned}\psi(x, z) &= \frac{d_{31}}{a_{33}} \left[\frac{du_0}{dx} + \frac{1}{2} \left(\frac{dw_0}{dx} \right)^2 + \frac{f_{14}}{d_{31}} \frac{d\phi}{dx} \right] z \\ &+ \frac{d_{31}}{a_{33}} \frac{d\phi}{dx} \frac{z^2}{2} + C_0\end{aligned}\quad (25)$$

$$\begin{aligned}H_z &= -\frac{\partial \psi}{\partial z} = -\frac{d_{31}}{a_{33}} \left[\frac{du_0}{dx} + \frac{1}{2} \left(\frac{dw_0}{dx} \right)^2 + z \frac{d\phi}{dx} \right] \\ &- \frac{f_{14}}{a_{33}} \frac{d\phi}{dx}\end{aligned}\quad (26)$$

Therefore, the higher-order stress and the component of classical stresses are determined as follows:

$$\begin{aligned}\sigma_{xx} &= \left(Q_{11} + \frac{d_{31}^2}{a_{33}} \right) \left[\frac{du_0}{dx} + \frac{1}{2} \left(\frac{dw_0}{dx} \right)^2 \right] \\ &+ \left(Q_{11} + \frac{d_{31}^2}{a_{33}} \right) z \frac{d\phi}{dx} - (Q_{11} + Q_{12}) \alpha \Delta T + \frac{f_{14} d_{31}}{a_{33}} \frac{d\phi}{dx}\end{aligned}\quad (27)$$

$$\sigma_{xz} = C_{55} \left(\frac{dw_0}{dx} + \phi \right) \quad (28)$$

$$\begin{aligned}\tau_{xxz} &= \left(g_{113113} + \frac{f_{14}^2}{a_{33}} \right) \frac{d\phi}{dx} \\ &+ \frac{f_{14} d_{31}}{a_{33}} \left[\frac{du_0}{dx} + \frac{1}{2} \left(\frac{dw_0}{dx} \right)^2 + z \frac{d\phi}{dx} \right]\end{aligned}\quad (29)$$

By substituting Eq. (27) into Eq. (23) and using Eq. (18) one can write:

$$u(x) = \frac{a_{33}}{A_{11}a_{33} + hd_{31}^2} \left(\int_0^x N_{xx}^T dx - \frac{hf_{14}d_{31}}{a_{33}} \phi \right) - \frac{1}{2} \int_0^x \left[\left(\frac{dw}{dx} \right)^2 - \left(\frac{dw^*}{dx} \right)^2 \right] dx + C_1x + C_2 \quad (30)$$

where w^* is the mid-plane initial rise. Using Eq. (30) and the essential boundary conditions of Eq. (22), the gradient of the axial displacement is obtained as:

$$\frac{du}{dx} = -\frac{hf_{14}d_{31}}{A_{11}a_{33} + hd_{31}^2} \frac{d\phi}{dx} - \frac{1}{2} \left[\left(\frac{dw}{dx} \right)^2 - \left(\frac{dw^*}{dx} \right)^2 \right] + \frac{a_{33}}{A_{11}a_{33} + hd_{31}^2} \left(N_{xx}^T - \frac{1}{a} \int_0^a N_{xx}^T dx \right) + \frac{1}{2a} \int_0^a \left[\left(\frac{dw}{dx} \right)^2 - \left(\frac{dw^*}{dx} \right)^2 \right] dx \quad (31)$$

Therefore, the stress resultants can be expressed as:

$$N_{xx} = \bar{N}_{xx} = \frac{A_{11}a_{33} + hd_{31}^2}{a_{33}} \frac{1}{2a} \int_0^a \left[\left(\frac{dw}{dx} \right)^2 - \left(\frac{dw^*}{dx} \right)^2 \right] dx - \frac{1}{a} \int_0^a N_{xx}^T dx \quad (32)$$

$$M_{xx} = \left(D_{11} + \frac{h^3 d_{31}^2}{12 a_{33}} \right) \frac{d\phi}{dx} - M_{xx}^T \quad (33)$$

$$N_{xxz} = \bar{g} \frac{d\phi}{dx} + \frac{hf_{14}d_{31}}{a_{33}} \frac{1}{2a} \int_0^a \left[\left(\frac{dw}{dx} \right)^2 - \left(\frac{dw^*}{dx} \right)^2 \right] dx + \frac{hf_{14}d_{31}}{A_{11}a_{33} + hd_{31}^2} \left(N_{xx}^T - \frac{1}{a} \int_0^a N_{xx}^T dx \right) \quad (34)$$

$$Q_x = K_s A_{55} \left(\frac{dw}{dx} - \frac{dw^*}{dx} + \phi \right) \quad (35)$$

where A_{11} , A_{55} , and D_{11} are given in Appendix A.

$$N_{xx}^T = \int_{-h/2}^{h/2} (Q_{11} + Q_{12}) \alpha \Delta T dz, \quad (36)$$

$$M_{xx}^T = \int_{-h/2}^{h/2} (Q_{11} + Q_{12}) \alpha \Delta T z dz,$$

$$\bar{g} = \hat{g}_{113113} + \frac{hf_{14}^2 A_{11}}{A_{11}a_{33} + hd_{31}^2}, \quad (37)$$

$$\hat{g}_{113113} = \int_{-h/2}^{h/2} g_{113113} dz = g_{113113} h$$

Using Eq. (18) and implementing NSG theory (Li and Hu 2017, Lim *et al.* 2015) into Eqs. (19) and (20) and then by substituting Eq. (32), the size-dependent governing differential equations of the shear deformable PM nanoplate strips by considering the DFM effect and geometrically imperfection are obtained as:

$$K_s A_{55} \left(\frac{d^2 w}{dx^2} - \frac{d^2 w^*}{dx^2} + \frac{d\phi}{dx} \right) - l^2 K_s A_{55} \left(\frac{d^4 w}{dx^4} - \frac{d^4 w^*}{dx^4} + \frac{d^3 \phi}{dx^3} \right) + \left(\frac{d^2 w}{dx^2} - \mu \frac{d^4 w}{dx^4} \right) \times \left\{ \frac{A_{11}a_{33} + hd_{31}^2}{a_{33}} \frac{1}{2a} \int_0^a \left[\left(\frac{dw}{dx} \right)^2 - \left(\frac{dw^*}{dx} \right)^2 \right] dx - \frac{1}{a} \int_0^a N_{xx}^T dx \right\} = 0 \quad (38)$$

$$-\frac{dM_{xx}^T}{dx} + \bar{D} \frac{d^2 \phi}{dx^2} - K_s A_{55} \left(\frac{dw}{dx} - \frac{dw^*}{dx} + \phi \right) \quad (39)$$

$$-l^2 \left[-\frac{d^3 M_{xx}^T}{dx^3} + \bar{D} \frac{d^4 \phi}{dx^4} - K_s A_{55} \left(\frac{d^3 w}{dx^3} - \frac{d^3 w^*}{dx^3} + \frac{d^2 \phi}{dx^2} \right) \right] = 0$$

where

$$\bar{D} = \bar{D} - \hat{g}_{113113} + \bar{g} = D_{11} + \frac{h^3 d_{31}^2}{12 a_{33}} + \bar{g} \quad (40)$$

The temperature distribution through the thickness of the plate is presented as below:

$$\Delta T(z) = \left(\frac{z + \frac{h}{2}}{h} \right)^n (T - T_0), \quad (41)$$

$$-h/2 \leq z \leq h/2, \quad 0 \leq n \leq \infty$$

Fig. 2 shows the uniform, linear, and parabolic temperature distributions through the thickness. By substituting Eq. (41) into Eq. (36), the thermal resultants are written as:

$$N_{xx}^T = A_T (T - T_0), \quad M_{xx}^T = D_T (T - T_0) \quad (42)$$

where $(T - T_0)$ is temperature rise from the reference temperature T_0 at which there is no thermal strains

$$A_T = \frac{Q_{11} \alpha (1 + \nu) h}{1 + n}, \quad D_T = \frac{Q_{11} \alpha (1 + \nu) h^2 n}{2(1 + n)(2 + n)} \quad (43)$$

Using Eq. (42), Eqs. (38) and (39) are simplified to

$$K_s A_{55} \left[\frac{d^2 w}{dx^2} - \frac{d^2 w^*}{dx^2} + \frac{d\phi}{dx} - l^2 \left(\frac{d^4 w}{dx^4} - \frac{d^4 w^*}{dx^4} + \frac{d^3 \phi}{dx^3} \right) \right] + \left(\frac{d^2 w}{dx^2} - \mu \frac{d^4 w}{dx^4} \right) \times \left\{ \frac{A_{11}a_{33} + hd_{31}^2}{a_{33}} \frac{1}{2a} \int_0^a \left[\left(\frac{dw}{dx} \right)^2 - \left(\frac{dw^*}{dx} \right)^2 \right] dx - N_{xx}^T \right\} = 0 \quad (44)$$

$$\bar{D} \left(\frac{d^2 \phi}{dx^2} - l^2 \frac{d^4 \phi}{dx^4} \right) - K_s A_{55} \left[\frac{dw}{dx} - \frac{dw^*}{dx} + \phi \right] - l^2 \left(\frac{d^3 w}{dx^3} - \frac{d^3 w^*}{dx^3} + \frac{d^2 \phi}{dx^2} \right) = 0 \quad (45)$$

2.5 Converse flexomagnetic effect

In this section the CFM effect is studied with the essential boundary conditions presented in Eq. (22), that is

$$\psi(x, z = h/2) = \Psi_1, \quad \psi(x, z = -h/2) = 0 \quad (46)$$

Substituting Eqs. (13) and (14) into Eq. (15) and combining with Eqs. (21) and (3) and then by applying the boundary conditions of Eq. (46), the magnetic potential and the z-component of the magnetic field vector are determined as:

$$\psi(x, z) = \frac{d_{31}}{2a_{33}} \left(z^2 - \frac{h^2}{4} \right) \frac{d\phi}{dx} + \frac{\Psi_1}{h} \left(z + \frac{h}{2} \right) \quad (47)$$

$$H_z = -z \frac{d_{31}}{a_{33}} \frac{d\phi}{dx} - \frac{\Psi_1}{h}$$

Similar to the procedure presented in section 2.4, the gradient of the axial displacement is obtained as:

$$\begin{aligned} \frac{du}{dx} &= \frac{1}{A_{11}}(N_{xx}^T - d_{31}\Psi_1) - \frac{1}{2} \left[\left(\frac{dw}{dx} \right)^2 - \left(\frac{dw^*}{dx} \right)^2 \right] \\ &+ \frac{1}{2a} \int_0^a \left[\left(\frac{dw}{dx} \right)^2 - \left(\frac{dw^*}{dx} \right)^2 \right] dx + \frac{d_{31}\Psi_1}{A_{11}} - \frac{1}{aA_{11}} \int_0^a N_{xx}^T dx \end{aligned} \quad (48)$$

and by considering the geometrical imperfection, the stress resultants are determined as follows:

$$\begin{aligned} N_{xx} &= \widehat{N}_{xx} = -\frac{1}{a} \int_0^a N_{xx}^T dx \\ &+ \frac{A_{11}}{2a} \int_0^a \left[\left(\frac{dw}{dx} \right)^2 - \left(\frac{dw^*}{dx} \right)^2 \right] dx + d_{31}\Psi_1 \\ M_{xx} &= -M_{xx}^T + \left(D_{11} + \frac{h^3 d_{31}^2}{12 a_{33}} \right) \frac{d\phi}{dx} \\ Q_x &= K_s A_{55} \left(\frac{dw}{dx} - \frac{dw^*}{dx} + \phi \right) \\ N_{xxz} &= \widehat{g}_{113113} \frac{d\phi}{dx} + f_{14}\Psi_1 \end{aligned} \quad (49)$$

Eqs. (A2), (36), and (37) are also valid for the DFM effect.

By applying the NSG theory to the equilibrium equations and considering the converse flexomagnetic effect and geometrical imperfection, the size-dependent governing differential equations of the shear deformable piezomagnetic nano-plate strips are obtained as:

$$\begin{aligned} K_s A_{55} \left(\frac{d^2 w}{dx^2} - \frac{d^2 w^*}{dx^2} + \frac{d\phi}{dx} \right) - l^2 K_s A_{55} \left(\frac{d^4 w}{dx^4} - \frac{d^4 w^*}{dx^4} + \frac{d^3 \phi}{dx^3} \right) \\ + \left(\frac{d^2 w}{dx^2} - \mu \frac{d^4 w}{dx^4} \right) \times \left\{ \frac{A_{11}}{2a} \int_0^a \left[\left(\frac{dw}{dx} \right)^2 - \left(\frac{dw^*}{dx} \right)^2 \right] dx \right. \\ \left. - \frac{1}{a} \int_0^a N_{xx}^T dx + d_{31}\Psi_1 \right\} = 0 \end{aligned} \quad (50)$$

$$\begin{aligned} -\frac{dM_{xx}^T}{dx} + \widehat{D} \frac{d^2 \phi}{dx^2} - K_s A_{55} \left(\frac{dw}{dx} - \frac{dw^*}{dx} + \phi \right) \\ - l^2 \left[-\frac{d^3 M_{xx}^T}{dx^3} + \widehat{D} \frac{d^4 \phi}{dx^4} - K_s A_{55} \left(\frac{d^3 w}{dx^3} - \frac{d^3 w^*}{dx^3} + \frac{d^2 \phi}{dx^2} \right) \right] = 0 \end{aligned} \quad (51)$$

When the temperature distribution is not the function of in-plane coordinates (i.e., Eq. (41)), Eqs. (50) and (51) can be written as:

$$\begin{aligned} K_s A_{55} \left[\frac{d^2 w}{dx^2} - \frac{d^2 w^*}{dx^2} + \frac{d\phi}{dx} - l^2 \left(\frac{d^4 w}{dx^4} - \frac{d^4 w^*}{dx^4} + \frac{d^3 \phi}{dx^3} \right) \right] \\ + \left(\frac{d^2 w}{dx^2} - \mu \frac{d^4 w}{dx^4} \right) \\ \times \left\{ \frac{A_{11}}{2a} \int_0^a \left[\left(\frac{dw}{dx} \right)^2 - \left(\frac{dw^*}{dx} \right)^2 \right] dx - N_{xx}^T + d_{31}\Psi_1 \right\} = 0 \end{aligned} \quad (52)$$

$$\begin{aligned} \widehat{D} \left(\frac{d^2 \phi}{dx^2} - l^2 \frac{d^4 \phi}{dx^4} \right) - K_s A_{55} \left[\begin{array}{c} \frac{dw}{dx} - \frac{dw^*}{dx} + \phi \\ -l^2 \left(\frac{d^3 w}{dx^3} - \frac{d^3 w^*}{dx^3} + \frac{d^2 \phi}{dx^2} \right) \end{array} \right] \\ = 0 \end{aligned} \quad (53)$$

3. Solution procedure

Analytical solution of the nonlinear governing differential equations of DFM and CFM effects is presented in this section. The transverse deflection, initial deflection,

and rotation of the nano-plate strip are considered as below:

$$\begin{aligned} w(x) &= \sum_{i=1}^{\infty} \widetilde{W} N_i(x), \quad w^*(x) = W^* h(x), \\ \phi(x) &= \sum_{i=1}^{\infty} \widetilde{\phi} \Theta_i(x) \end{aligned} \quad (54)$$

where N_i , h , and Θ_i are the shape functions which for the case of simply supported end conditions are presented as follows (Barati and Zenkour 2019, Malikan *et al.* 2020):

$$\begin{aligned} N_i(x) &= \sin\left(\frac{i\pi x}{a}\right), \quad h(x) = \sin\left(\frac{\pi x}{a}\right), \\ \Theta_i(x) &= \cos\left(\frac{i\pi x}{a}\right) \end{aligned} \quad (55)$$

By multiplying the residuals of the governing equations by the appropriate shape functions and then integrating over the length of the plate strip, one can obtain the following nonlinear equations:

$$P_1 \widetilde{W} + M_1 W^* + N_1 \widetilde{\phi} + K_1 \widetilde{W}^3 + G_1 \widetilde{W} W^{*2} = 0 \quad (56)$$

$$P_2 \widetilde{W} + M_2 W^* + N_2 \widetilde{\phi} = 0 \quad (57)$$

where the coefficients of the above equations in case of the DFM and CFM effects are defined in Appendix A.

After some mathematical manipulations, the closed-form solution of the post-buckling load-deflection relationship is presented for the simply supported case for the DFM effect as:

$$\begin{aligned} N^{Mech} &= \frac{\overline{D} \alpha_i^2 \lambda_{li} \widetilde{W} - W^*}{\Lambda_1 \lambda_{\mu i} \widetilde{W}} \\ &+ \frac{A_{11} a_{33} + h d_{31}^2}{4 a_{33}} \alpha_i^2 (\widetilde{W}^2 - W^{*2}) - N_{xx}^T \end{aligned} \quad (58)$$

and, for the CFM effect the closed-form solution is:

$$\begin{aligned} N^{Mech} &= \frac{\overline{D} \alpha_i^2 \lambda_{li} \widetilde{W} - W^*}{\Lambda_2 \lambda_{\mu i} \widetilde{W}} + \frac{A_{11}}{4} \alpha_i^2 (\widetilde{W}^2 - W^{*2}) \\ &+ d_{31}\Psi_1 - N_{xx}^T \end{aligned} \quad (59)$$

where

$$\begin{aligned} \alpha_i &= \frac{i\pi}{a}, \quad \lambda_{li} = (1 + l^2 \alpha_i^2), \quad \lambda_{\mu i} = (1 + \mu \alpha_i^2), \\ \Lambda_1 &= 1 + \frac{\overline{D} \alpha_i^2}{K_s A_{55}}, \quad \Lambda_2 = 1 + \frac{\overline{D} \alpha_i^2}{K_s A_{55}} \end{aligned} \quad (60)$$

In the linear case and without geometrical imperfection, Eqs. (58) and (59) can be expressed as:

$$N^{Mech} = \frac{\overline{D} \alpha_i^2 \lambda_{li}}{\Lambda_1 \lambda_{\mu i}} - N_{xx}^T \quad (61)$$

$$N^{Mech} = \frac{\overline{D} \alpha_i^2 \lambda_{li}}{\Lambda_2 \lambda_{\mu i}} + d_{31}\Psi_1 - N_{xx}^T \quad (62)$$

4. Validation

For Timoshenko beams without considering the PFM effects, the critical buckling load in Eqs. (61) and (62) can

Table 1 Comparison of nondimensional critical buckling loads $\bar{N}_{cr} = N \times (L^2/EI)$ of simply-supported Timoshenko nanobeams

$e_0 a$ (nm)	CBL	L/h=10			L/h=50		
		l=0 nm	l=1 nm	l=2 nm	l=0 nm	l=1 nm	l=2 nm
0	Lu <i>et al.</i> (2017b)	9.6227	10.5724	13.4216	9.8595	9.8984	10.0152
	Present (Eq. 58)	9.6227	10.5724	13.4216	9.8595	9.8984	10.0152
	Present (Eq. 59)	9.6227	10.5724	13.4216	9.8595	9.8984	10.0152
1	Lu <i>et al.</i> (2017b)	8.7583	9.6227	12.2159	9.8207	9.8595	9.9758
	Present (Eq. 58)	8.7583	9.6227	12.2159	9.8207	9.8595	9.9758
	Present (Eq. 59)	8.7583	9.6227	12.2159	9.8207	9.8595	9.9758
2	Lu <i>et al.</i> (2017b)	6.8990	7.5800	9.6227	9.7062	9.7445	9.8595
	Present (Eq. 58)	6.8990	7.5800	9.6227	9.7062	9.7445	9.8595
	Present (Eq. 59)	6.8990	7.5800	9.6227	9.7062	9.7445	9.8595

Table 2 Comparison of nondimensional post-buckling load to non-dimensional buckling load ratio (λ_{NL}/λ_L) of simply-supported Timoshenko beams ($\nu = 0.3, K_s = 5/6, \bar{W}/r = 1.0$)

	Present Eqs. (58) and (59)	Gunda (2014)
$\beta = 25$	1.2623	1.2623
$\beta = 50$	1.2531	1.2531
$\beta = 100$	1.2508	1.2508
$\beta \rightarrow \infty$	1.25	1.25

Table 3 Magneto-mechanical coefficients of material properties (Malikan *et al.* 2021, Pan and Han 2005)

CoFe ₂ O ₄
$E = 286 \text{ GPa}, \nu = 0.32$
$d_{31} = 580.3 \text{ N/(A.m)}, a_{33} = 157 \times 10^{-6} \text{ N/A}^2$
$f_{14} = 10^{-9} \text{ N/A}, h = 1 \text{ nm}$
$\alpha = 11.8 \times 10^{-6} \text{ 1/K}$

can be simplified to that derived by Xu and Zheng (2019). By ignoring the strain gradient parameter ($l = 0$) and without the PFM effects, the critical buckling load in Eqs. (61) and (62) can be simplified to that derived by Reddy (2007).

For Euler-Bernoulli (EB) beams without considering the PFM effects and geometrical imperfection, the critical buckling and post-buckling loads in Eqs. (58) and (59) can be simplified to that derived by Li and Hu (2017). By ignoring the nonlocal and strain gradient parameters ($\mu = l = 0$) and without geometrical imperfection and the PFM effects, the critical buckling and post-buckling loads by Eqs. (58) and (59) can be simplified to that derived by Gupta *et al.* (2010). Note that, in case of EB theory, $\Lambda_1 = \Lambda_2 = 1$.

Furthermore, to verify the efficiency and accuracy of the present model, some numerical results are tabulated and compared with those existing in the literature. In Table 1, dimensionless linear buckling loads of the strip without geometrical imperfection and the PFM effects are presented. The material properties used in Table 1 are $E = 30 \times 10^6$ si and $\nu = 0.3$. The ratio of dimensionless post-buckling

loads to dimensionless linear buckling loads of the strip without geometrical imperfection and the PFM effects are presented in Table 2. In this table, $\beta = L/r$ is the slenderness ratio of the beam, r is the radius of gyration, and $\lambda_L = (P_L L^2)/EI$ and $\lambda_{NL} = (P_{NL} L^2)/EI$ are, respectively, dimensionless buckling and post-buckling loads.

5. Numerical results and discussion

In this section, various numerical results are presented. The effects of numerous parameters on buckling and post-buckling loads are investigated. The material properties for numerical investigations are listed in Table 3 and are used in the present study, unless otherwise stated.

Table 4 presents a comparison between critical buckling loads (linear) and post-buckling loads (nonlinear) of strips under uniform, linear, and nonlinear temperature distributions for different slenderness ratios. In both direct and converse flexomagnetic effects, the nonlinear temperature distribution increases the values of the buckling and post-buckling loads while the slenderness ratio has the opposite effect. In case

Table 4 Comparison of buckling and post-buckling loads of PFM nano-plate strip ($\bar{W}/h = 0.1, W^* = 0, l/h = 1, e_0a/h = 1, \Psi_1 = 1 \text{ mA}, T - T_0 = 100 \text{ K}$)

Temperature distribution		P_L			P_{NL}		
		L/h=10	L/h=20	L/h=50	L/h=10	L/h=20	L/h=50
DFM	Uniform ($\varphi=0$)	2.0670	0.1585	-0.3909	2.1462	0.1783	-0.3877
	Linear ($\varphi=1$)	2.3152	0.4066	-0.1427	2.3943	0.4264	-0.1396
	Nonlinear($\varphi=2$)	2.3979	0.4893	-0.0600	2.4771	0.5091	-0.0569
CFM	Uniform ($\varphi=0$)	2.6473	0.7388	0.1894	2.7260 (2.973%)*	0.7584 (2.653%)	0.1926 (1.690%)
	Linear ($\varphi=1$)	2.8955	0.9869	0.4376	2.9741 (2.715%)	1.0066 (1.996%)	0.4407 (0.708%)
	Nonlinear($\varphi=2$)	2.9782	1.0696	0.5203	3.0568 (2.639%)	1.0893 (1.842%)	0.5234 (0.596%)

*Discrepancy between the buckling and post-buckling loads ($\frac{2.7260-2.6473}{2.6473} \times 100\%$)

Table 5 Dimensionless size-dependent buckling ratio (P_{NL}/P_L) of PFM nano-plate strips ($W^* = 0, l = 1 \times 10^{-9}, e_0a = 1 \times 10^{-9}, \Psi_1 = 0 \text{ mA}, T - T_0 = 0$)

\bar{W}/h	DFM			CFM		
	L/h=10	L/h=20	L/h=50	L/h=10	L/h=20	L/h=50
0	1.0000	1.0000	1.0000	1.0000	1.0000	1.0000
0.1	1.0309	1.0302	1.0300	1.0307	1.0300	1.0298
0.2	1.1235	1.1209	1.1201	1.1227	1.1201	1.1193
0.3	1.2779	1.2720	1.2703	1.2760	1.2702	1.2685
0.4	1.4940	1.4835	1.4806	1.4907	1.4803	1.4773
0.5	1.7719	1.7555	1.7509	1.7668	1.7504	1.7459

Table 6 Effect of strain gradient on linear and nonlinear buckling loads of PFM nano-plate strips ($T - T_0 = 0, \Psi_1 = 1 \text{ mA}, W^* = 0, L/h = 10$)

	$e_0a/h = 0$			$l/h = 0$		
	$\frac{l}{h}$	DFM	CFM	$\frac{e_0a}{h}$	DFM	CFM
	$\bar{W}/h = 0$ (Linear case)	0	2.5633	3.1436	0	2.5633
0.5		2.6266 (+2.47%)	3.2069 (+2.01%)	0.5	2.5016 (-2.407%)	3.0819 (-1.96%)
1.0		2.8163 (+9.87%)*	3.3966 (+8.05%)	1.0	2.3331 (-8.981%)	2.9134 (-7.32%)
$\bar{W}/h = 0.5$	0	4.5420	5.1091	0	4.5420	5.1091
	0.5	4.6053 (+1.39%)	5.1723 (+1.24%)	0.5	4.4803 (-1.36%)	5.0474 (-1.21%)
	1.0	4.7950 (+5.57%)	5.3621 (+4.95%)	1.0	4.3118 (-5.07%)	4.8788 (-4.51%)
$\bar{W}/h = 1$	0	10.4781	11.0055	0	10.4781	11.0055
	0.5	10.5413 (+0.60%)	11.0687 (+0.57%)	0.5	10.4164 (-0.59%)	10.9437 (-0.56%)
	1.0	10.7311 (+2.41%)	11.2584 (+2.30%)	1.0	10.2478 (-2.20%)	10.7752 (-2.09%)

* $\frac{(2.8163-2.5633)}{2.5633} \times 100\%$

of the CFM effect, at a constant slenderness ratio, the minimum discrepancy between the buckling and post-buckling loads occurs at nonlinear thermal loads. Also, by increasing the length of the plate strip, the difference between the buckling and post-buckling loads reduces. It is remarked that by increasing the ratio of length to thickness of nano-plate strip to 50, the critical and post-buckling loads take a negative value, thus, buckling occurs for traction

loads instead of compression. It should be noted that the differences between the buckling resistances under direct and converse FM effects are due to a non-zero increment in the buckling load that is induced by the external magnetic potential. This response to an external magnetic potential is the CFM effect, in line with the converse piezomagnetic effect causing an additional term due to the external magnetic potential. Table 5 shows the effect of dimensionless

Table 7 Buckling and post-buckling loads of PFM nano-plate strips for different magnetic potentials and size-effect parameters ($T - T_0 = 0$, $W^* = 0$, $L/h = 10$, $\tilde{W}/h = 0.5$)

l/h	$e_0 a/h$	P_L			P_{NL}		
		$\Psi_1 = -2 \text{ mA}$	$\Psi_1 = 0 \text{ mA}$	$\Psi_1 = 2 \text{ mA}$	$\Psi_1 = -2 \text{ mA}$	$\Psi_1 = 0 \text{ mA}$	$\Psi_1 = 2 \text{ mA}$
0	0	1.4027	2.5633	3.7239	3.3682	4.5288	5.6894
	0.5	1.3410	2.5016	3.6622	3.3065	4.4671	5.6277
	1	1.1725	2.3331	3.4937	3.1379	4.2985	5.4591
0.5	0	1.4660	2.6266	3.7872	3.4314	4.5920	5.7526
	0.5	1.4027	2.5633	3.7239	3.3682	4.5288	5.6894
	1	1.2300	2.3906	3.5512	3.1955	4.3561	5.5167
1	0	1.6557	2.8163	3.9769	3.6212	4.7818	5.9424
	0.5	1.5879	2.7485	3.9091	3.5534	4.7140	5.8746
	1	1.4027	2.5633	3.7239	3.3682	4.5288	5.6894

Table 8 Effect of flexomagneticity and size-effect parameters on dimensionless buckling ratio (P_{NL}/P_L) of piezomagnetic nano-plate strips under direct FM effect. ($T - T_0 = 0$, $W^* = 0$, $\tilde{W}/h = 0.5$, $L/h = 5$)

$e_0 a/h$	Without flexomagneticity			With flexomagneticity ($f_{14} = 10^{-9} \text{ N/A}$)			With flexomagneticity ($f_{14} = 10^{-7} \text{ N/A}$)		
	$l/h = 0$	$l/h = 1$	$l/h = 2$	$l/h = 0$	$l/h = 1$	$l/h = 2$	$l/h = 0$	$l/h = 1$	$l/h = 2$
0	1.8377	1.6006	1.3248	1.8377	1.6006	1.3248	1.8359 (-0.098%)*	1.5993 (-0.081%)	1.3241 (-0.053%)
1	2.1684	1.8377	1.4530	2.1684	1.8377	1.4530	2.1659 (-0.115%)	1.8359 (-0.098%)	1.4521 (-0.062%)
2	3.1605	2.5490	1.8377	3.1605	2.5490	1.8377	3.1559 (-0.145%)	2.5457 (-0.129%)	1.8359 (-0.098%)

* $\frac{(1.8359 - 1.8377)}{1.8377} \times 100\%$

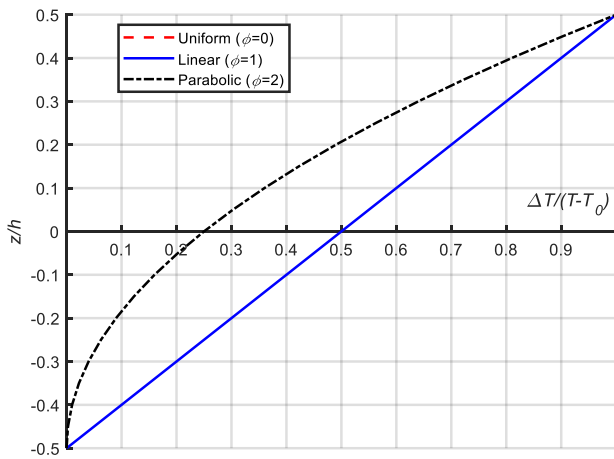


Fig. 2 The uniform, linear, and parabolic temperature distributions through the thickness

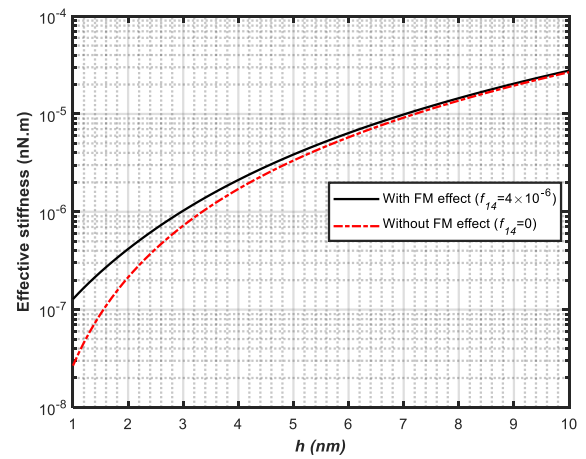


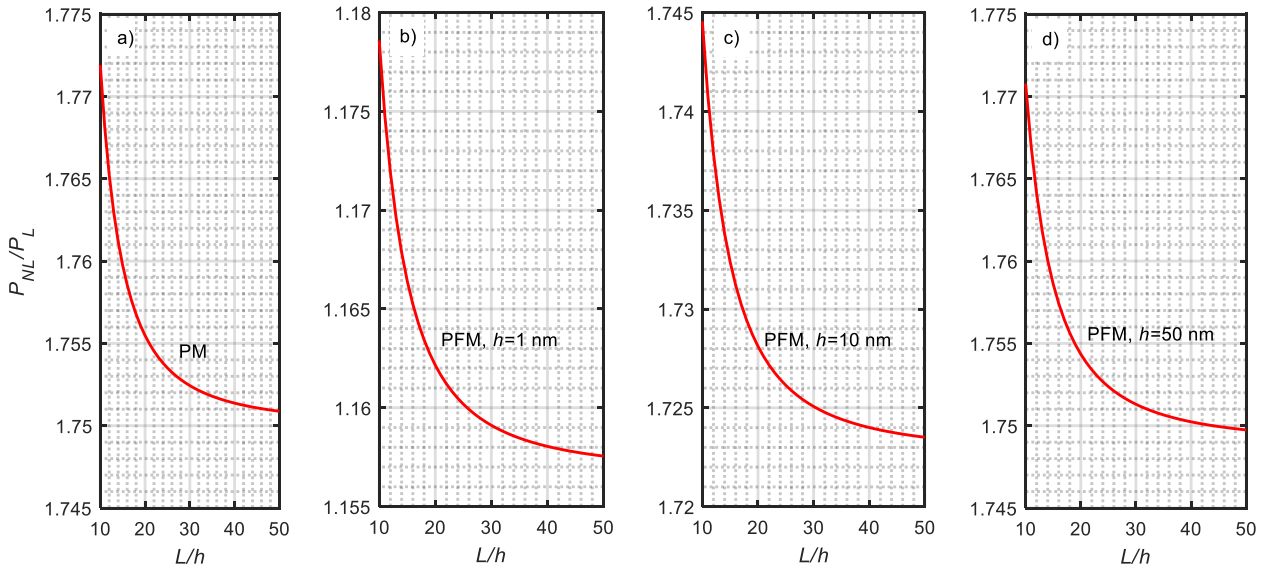
Fig. 3 The effective stiffness of PM nano-plate strips with and without FM effect vs. thickness

(\tilde{W}/h) on the dimensionless buckling load ratio (P_{NL}/P_L) considering the size-dependency. By increasing the maximum deflection, the dimensionless buckling load ratio increases while the slenderness ratio has the opposite effect. In Table 6, the size-dependent in-plane loads associated with different dimensionless amplitudes are tabulated for PFM nano-plate strips with both direct and converse effects corresponding to various values of the strain gradient and nonlocal parameters. It is shown that by moving to a deeper part of the post-buckling domain, the role of both strain

gradient and non-local parameters decreases.

Table 7 shows the buckling and post-buckling loads of PFM nano-plate strips for different values of applied magnetic potentials and size-effect parameters. It is demonstrated that as the strain gradient parameter increases, the values of the linear and nonlinear loads increase while the nonlocal parameter has the opposite effect. It is also shown that the buckling and post-buckling loads increase as the externally applied magnetic potential is increased.

Table 8 shows the effect of flexomagneticity and size-



(a) The piezomagnetics

(b)-(d) The flexomagnetics

Fig. 4 Dimensionless buckling ratio vs. slenderness ratio and thickness ($f_{14} = 4 \times 10^{-6}$, $e_0a = h$, $l = h$, $W^* = 0$, $\tilde{W} = 0.5h$, $T - T_0 = 0$, $\Psi_1 = 0$)

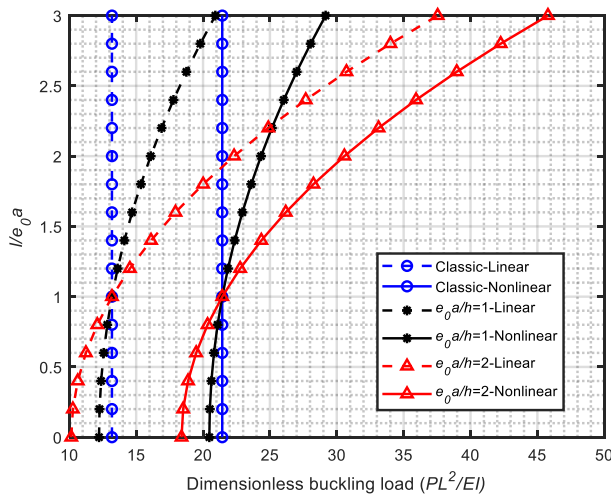


Fig. 5 Effect of nonlocal and strain gradient parameters on the non-dimensional buckling and post-buckling loads of PFM nano-plate strips

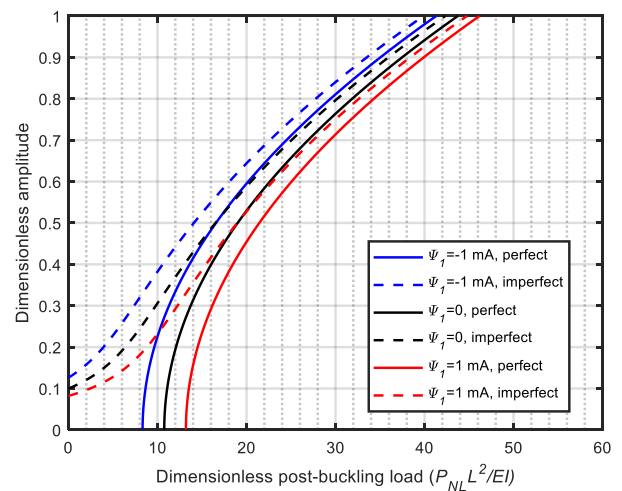


Fig. 6 Post-buckling path at different magnetic fields for the CFM case

effect parameters on dimensionless buckling ratio of piezomagnetic nano-plate strips under direct FM effect. As the dimensionless strain gradient parameter increases, the buckling ratio and the role of flexomagnetics decrease. Also, it is demonstrated that the buckling ratio and the role of flexomagnetics increase by increasing the nonlocality.

Using Eq. (40), the effective flexural stiffness of PM and PFM nano-plate strips versus the thickness is demonstrated in Fig. 3. It is seen that the effective stiffness obtained by the classical piezomagnetics theory is smaller than that calculated from the current theory for small thicknesses. Also, increasing the thickness decreases the differences between the two theories. This result affirms that the FM effect is more significant at small scales.

The effect of the flexomagnetics on the dimensionless buckling ratio is studied in Fig. 4. The buckling load ratio

predicted by the FM effect is smaller than that calculated by the PM effect. By increasing the thickness of the PFM nano-plate strips, the effect of FM decreases, and the difference between the values predicted by the PM model and the PFM model is much smaller and so the flexomagnetics can be neglected. Figs. 3 and 4 affirm the size-dependency of the flexomagnetic effect.

Buckling and post-buckling behaviors of piezomagnetic nano-plate strips with converse FM effect are demonstrated in Fig. 5 for ($T - T_0 = 0$, $L/h = 10$, $W^* = 0$, $\tilde{W} = 0.5h$, $\Psi_1 = 1 \text{ mA}$). At a constant nonlocal parameter, increasing the strain gradient parameter leads to increasing the dimensionless buckling and post-buckling loads, and the PFM nano-plate strips will be stiffer. The linear and nonlinear buckling behaviors of the simply supported PFM nano-plate strips show a stiffness-softening effect for $e_0a > l$, and a stiffness-hardening effect for $e_0a < l$.

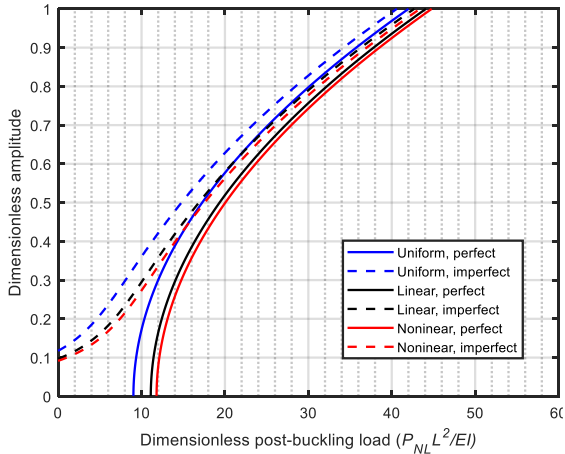


Fig. 7 Post-buckling path at 200 K and various temperature distribution for the CFM case

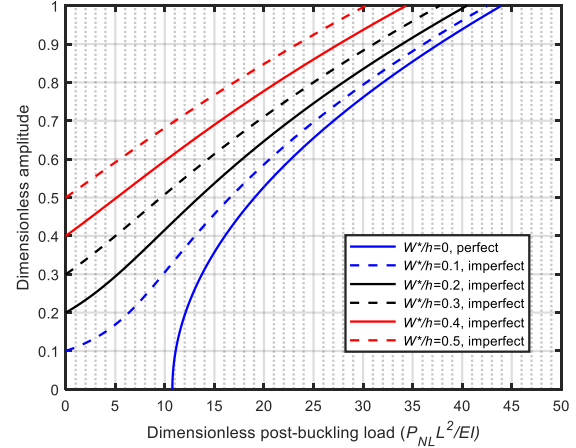


Fig. 9 Equilibrium paths of nonlinear buckling of size-dependent PFM nano-plate strips with geometrical imperfection for the DFM case

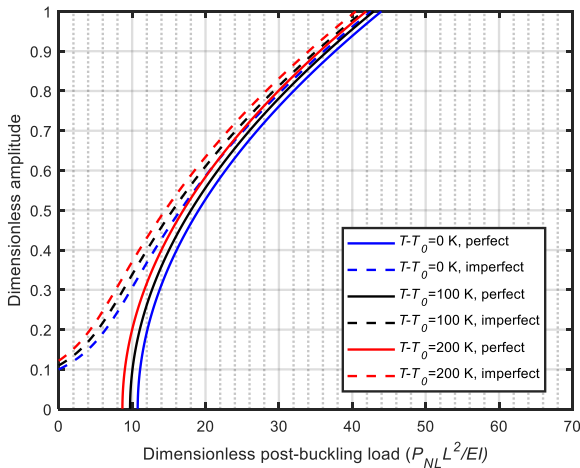


Fig. 8 Post-buckling path at different temperatures and linear thermal environment for the DFM case

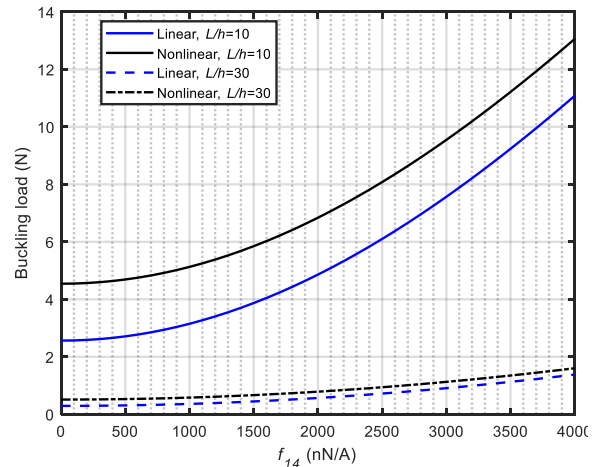


Fig. 10 Buckling and post-buckling loads vs. flexomagnetic coefficient at different slenderness ratios for the DFM case

The effects of magnetic potential and geometrical imperfection on the nondimensional nonlinear buckling load of PM nano-plate strips with CFM effect are indicated in Fig. 6 at $e_0 a = l = h, W^* = 0.1h$. Positive values of the magnetic potential increase the post-buckling load in both perfect and imperfect configurations. As expected, the post-buckling load grows as \tilde{W}/h is increased. In case of perfect nano-plate strips, the critical buckling load corresponds to zero amplitude $\tilde{W}/h = 0$, and in case of nano-plate strips with the initial rise (imperfect), there is no critical load.

The effect of temperature distribution on dimensionless post-buckling behavior of PFM nano-plate strips is indicated in Fig. 7 ($L/h = 10, e_0 a = l = h, W^* = 0.1h, \Psi_1 = 1 \text{ mA}, T - T_0 = 200 \text{ K}$). It can be seen that by increasing the dimensionless amplitude, the values of the dimensionless post-buckling loads in both perfect and imperfect configurations get closer. This is due to that increasing the dimensionless amplitude decreases the contribution of the mid-plane initial rise. When the temperature distribution varies from uniform to nonlinear regime, the thermal forces reduce, therefore the nonlinear buckling load increases.

To study the effect of temperature on buckling load, linear distribution of temperature is used in Fig. 8 ($L/h = 10, e_0 a = l = h, W^* = 0.1h$). It is well-known that the larger values of temperature increase the thermal forces, therefore, as illustrated in Fig. 8 the dimensionless post-buckling load decreases.

The effect of the mid-plane initial rise (imperfection) is studied in Fig. 9 ($L/h = 10, e_0 a = l = h, T - T_0 = 0$). As illustrated in this figure, there is no critical buckling load for the case of imperfect PFM nano-plate strips, and the nano-plate strip is at its initial configuration. It means that the starting point of an imperfect nano-plate strip, the critical buckling load is zero.

The effect of the flexomagnetic coefficient on the linear and nonlinear buckling loads at different slenderness ratios is presented in Fig. 10 ($e_0 a = l = h, W^* = 0, T - T_0 = 0, \tilde{W}/h = 0.5$). Increasing the FM coefficient leads to increasing the stiffness and, therefore, increasing the buckling loads. Also, decreasing the slenderness ratio has a similar effect, increasing the stiffness and buckling loads. From this figure, it can be seen that by increasing the

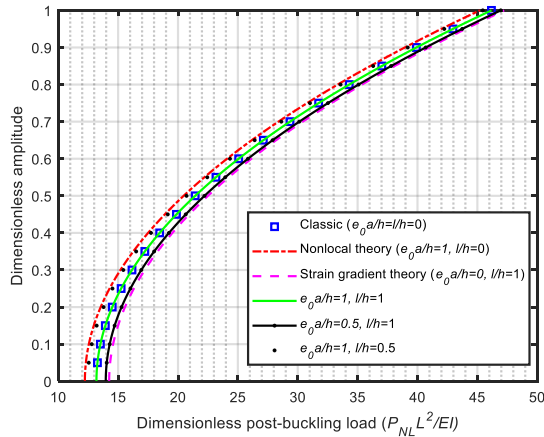


Fig. 11 Dimensionless post-buckling loads vs. dimensionless amplitude at different small-scale parameters for the CFM case

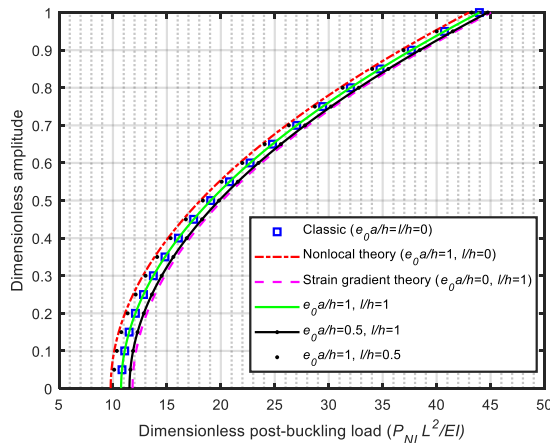


Fig. 12 Dimensionless post-buckling loads vs. dimensionless amplitude at different small-scale parameters for DFM case

slenderness ratio, the discrepancy between linear and nonlinear buckling loads decreases, which means at large values of slenderness ratios, the failure of the material occurs faster.

The effect of the nonlocality and the strain gradient parameter on the nonlinear post-buckling behavior of the PFM nano-plate strips is studied in Figs. 11 and 12 for direct and converse FM effects, respectively. It is seen that the curves converge as the dimensionless amplitude is increased. It means that the role of small-scale parameters reduces. Also, one can find that the nonlocal and strain gradient parameters increase or decrease the stiffness depending on the relation between the scale parameters. The stiffness-softening and stiffness-hardening can be found when $e_0 a > l$ and $e_0 a < l$, respectively. It is important to note that in case of $e_0 a = l$, there are no stiffness-softening and stiffness-hardening effects.

6. Conclusions

Linear and nonlinear buckling behaviors of piezomagnetic nano-plate strips considering the direct and

converse flexomagnetic effects are studied. The first-order shear deformation plate theory combining with the von-Kármán strains is used. The Nonlocal strain gradient theory is used to take into account the effect of size. The governing differential equations of equilibrium and associated boundary conditions are derived based on a variational method. A closed-form solution is presented and the effects of vital parameters such as imperfection, magnetic field, temperature, temperature distribution, and the scaling parameters with and without the flexomagnetic effect are studied. It was found that nonlinear thermal loads and larger slenderness ratio, decreases the difference between the buckling and post-buckling loads and the nonlinear buckling load increases as the temperature distribution varies from uniform to nonlinear regime. Increasing the thickness, decreases the discrepancy between the effective stiffness of a PM and PFM nano-plate strips and the flexomagneticity can be negligible. At the starting point of deflection, the geometrical imperfection has an enormous influence on the post-buckling path. By moving to deeper parts of post-buckling region the role of small-scale parameters and geometrical imperfection reduces. Depending on the relation between the scaling parameters, the linear and nonlinear buckling behaviors of the simply supported PFM nano-plate strips show a stiffness-softening or a stiffness-hardening effect. Also, increasing the FM coefficient leads to increasing the stiffness. The nonlocality causes the stiffness-softening and reduces the post-buckling load while the strain gradient parameter has the opposite influence. Positive values of the magnetic potential increase the post-buckling load in both perfect and imperfect configurations. In case of nano-plate strips with geometrical imperfection there is no critical load.

References

- Asrari, R., Ebrahimi, F. and Kheirikhah, M.M. (2020), "On post-buckling characteristics of functionally graded smart magneto-electro-elastic nanoscale shells", *Adv. Nano Res.*, **9**(1), 33-45. <https://doi.org/10.12989/anr.2020.9.1.033>.
- Bagheri, R. and Tadi Beni, Y. (2021), "On the size-dependent nonlinear dynamics of viscoelastic/flexoelectric nanobeams", *J. Vib. Control*, **27**(17-18), 2018-2033. <https://doi.org/10.1177/1077546320952225>.
- Barati, M.R. and Zenkour, A.M. (2019), "Thermal post-buckling analysis of closed circuit flexoelectric nanobeams with surface effects and geometrical imperfection", *Mech. Adv. Mater. Struct.*, **26**(17), 1482-1490. <https://doi.org/10.1080/15376494.2018.1432821>.
- Belyaev, B.A., Izotov, A.V., Solovev, P.N. and Boev, N.M. (2020), "Strain-gradient-induced unidirectional magnetic anisotropy in nanocrystalline thin permalloy films", *Physica Status Solidi (RRL)*, **14**(1), 1900467. <https://doi.org/10.1002/pssr.201900467>.
- Cai, R., Antohe, V.A., Nysten, B., Piriaux, L. and Jonas, A.M. (2020), "Thermally induced flexo-type effects in nanopatterned multiferroic layers", *Adv. Funct. Mater.*, **30**(14), 1910371. <https://doi.org/10.1002/adfm.201910371>.
- Eliseev, E.A., Morozovska, A.N., Glinchuk, M.D. and Blinc, R. (2009), "Spontaneous flexoelectric/flexomagnetic effect in nanoferroics", *Phys. Rev. B*, **79**(16), 165433. <https://link.aps.org/doi/10.1103/PhysRevB.79.165433>.

- Eliseev, E.A., Glinchuk, M.D., Khist, V., Skorokhod, V.V., Blinc, R. and Morozovska, A.N. (2011), "Linear magnetoelectric coupling and ferroelectricity induced by the flexomagnetic effect in ferroics", *Phys. Rev. B*, **84**(17), 174112. <https://link.aps.org/doi/10.1103/PhysRevB.84.174112>.
- Eliseev, E.A., Morozovska, A.N., Khist, V.V. and Polinger, V. (2019), *Chapter Six- Effective Flexoelectric and Flexomagnetic Response of Ferroics In Solid State Physics*, **70**, 237-289, Academic Press, Massachusetts, U.S.A.
- Fahrner, W.R. (2005), *Nanotechnology and Nanoelectronics: Materials, Devices, Measurement Techniques*, Springer, Berlin, Germany.
- Fenjan, R.M., Hamad, L.B. and Faleh, N.M. (2020), "Mechanical-hygro-thermal vibrations of functionally graded porous plates with nonlocal and strain gradient effects", *Adv. Aircr. Spacecr.*, **7**(2), 169-186. <https://doi.org/10.12989/aas.2020.7.2.169>.
- Gunda, J.B. (2014), "Thermal post-buckling and large amplitude free vibration analysis of Timoshenko beams: Simple closed-form solutions", *Appl. Math. Model.*, **38**(17-18), 4548-4558. <https://doi.org/10.1016/j.apm.2014.02.019>.
- Gupta, R., Gunda, J.B., Ranga Janardhan, G. and Venkateswara, R.G. (2010), "Post-buckling analysis of composite beams: Simple and accurate closed-form expressions", *Compos. Struct.*, **92**(8), 1947-1956. <https://doi.org/10.1016/j.compstruct.2009.12.010>.
- Kundalwal, S.I. and Ray, M.C. (2016), "Smart damping of fuzzy fiber reinforced composite plates using 1-3 piezoelectric composites", *J. Vib. Control.*, **22**(6), 1526-1546. <https://doi.org/10.1177/1077546314543726>.
- Kundalwal, S.I., Shingare, K.B. and Rathi, A. (2019), "Effect of flexoelectricity on the electromechanical response of graphene nanocomposite beam", *Int. J. Mech. Mater. Des.*, **15**(3), 447-470. <https://doi.org/10.1007/s10999-018-9417-6>.
- Lee, D., Yoon, A., Jang, S.Y., Yoon, J.G., Chung, J.S., Kim, M., Scott, J.F. and Noh, T.W. (2011), "Giant flexoelectric effect in ferroelectric epitaxial thin films", *Phys. Rev. Lett.*, **107**(5), 057602. <https://doi.org/10.1103/PhysRevLett.107.057602>.
- Li, L. and Hu, Y. (2017), "Post-buckling analysis of functionally graded nanobeams incorporating nonlocal stress and microstructure-dependent strain gradient effects", *Int. J. Mech. Sci.*, **120**, 159-170. <https://doi.org/10.1016/j.ijmecsci.2016.11.025>.
- Lim, C., Zhang, G. and Reddy, J. (2015), "A higher-order nonlocal elasticity and strain gradient theory and its applications in wave propagation", *J. Mech. Phys. Solids*, **78**, 298-313. <https://doi.org/10.1016/j.jmps.2015.02.001>.
- Lu, L., Guo, X. and Zhao, J. (2017b), "A unified nonlocal strain gradient model for nanobeams and the importance of higher order terms", *Int. J. Eng. Sci.*, **119**, 265-277. <https://doi.org/10.1016/j.ijengsci.2017.06.024>.
- Lukashev, P. and Sabirianov, R.F. (2010), "Flexomagnetic effect in frustrated triangular magnetic structures", *Phys. Rev. B*, **82**(9), 094417. <https://doi.org/10.1103/PhysRevB.82.094417>.
- Malikan, M. and Eremeyev, V.A. (2021a), "Flexomagnetic response of buckled piezomagnetic composite nanoplates", *Compos. Struct.*, **267**, 113932. <https://doi.org/10.1016/j.compstruct.2021.113932>.
- Malikan, M. and Eremeyev, V.A. (2021b), "Flexomagneticity in buckled shear de-formable hard-magnetic soft structures", *Continuum Mech. Therm.*, **34**(1), 1-16. <https://doi.org/10.1007/s00161-021-01034-y>.
- Malikan, M., Uglov, N.S. and Eremeyev, V.A. (2020), "On instabilities and post-buckling of piezomagnetic and flexomagnetic nanostructures", *Int. J. Eng. Sci.*, **157**, 103395. <https://doi.org/10.1016/j.ijengsci.2020.103395>.
- Malikan, M., Wiczenbach, T. and Eremeyev, V.A. (2021), "On thermal stability of piezo-flexomagnetic microbeams considering different temperature distributions", *Continuum Mech. Therm.*, **33**(4), 1281-1297. <https://doi.org/10.1007/s00161-021-00971-y>.
- Mir, M. and Tahani, M. (2020), "Graphene-based mass sensors: Chaotic dynamics analysis using the nonlocal strain gradient model", *Appl. Math. Model.*, **81**, 799-817. <https://doi.org/10.1016/j.apm.2020.01.022>.
- Mirjavadi, S.S., Forsat, M., Barati, M.R., Abdella, G.M., Hamouda, A.M.S., Afshari, B.M. and Rabby, S. (2019), "Post-buckling analysis of piezo-magnetic nanobeams with geometrical imperfection and different piezoelectric contents", *Microsyst. Technol.*, **25**(9), 3477-3488. <https://doi.org/10.1007/s00542-018-4241-3>.
- Mohamed, N., Eltahir, M.A., Mohamed, S.A. and Seddek, L.F. (2019), "Energy equivalent model in analysis of postbuckling of imperfect carbon nanotubes resting on nonlinear elastic foundation", *Struct. Eng. Mech.*, **70**(6), 737-750. <https://doi.org/10.12989/sem.2019.70.6.737>.
- Moosavi, S.M., Sarani, Z., Chia, C.H., Gan, S., Azahari, N.A. and Kaco, H. (2017), "Hydrothermal synthesis, magnetic properties and characterization of CoFe₂O₄ nanocrystals", *Ceram. Int.*, **43**(10), 7889-7894. <https://doi.org/10.1016/j.ceramint.2017.03.110>.
- Moradi, R., Radhi, A. and Behdinin, K. (2020), "Damped dynamic behavior of an advanced piezoelectric sandwich plate", *Compos. Struct.*, **243**, 112243. <https://doi.org/10.1016/j.compstruct.2020.112243>.
- Pan, E. and Han, F. (2005), "Exact solution for functionally graded and layered magneto-electro-elastic plates", *Int. J. Eng. Sci.*, **43**(3-4), 321-339. <https://doi.org/10.1016/j.ijengsci.2004.09.006>.
- Pyatakov, A.P. and Zvezdin, A.K. (2009), "Flexomagnetolectric interaction in multiferroics", *Eur. Phys. J. B*, **71**(3), 419-427. <https://doi.org/10.1140/epjb/e2009-00281-5>.
- Radgolchin, M. and Tahani, M. (2021), "Nonlinear vibration analysis of beam microgyroscopes using nonlocal strain gradient theory", *Sens. Imag.*, **22**(1), 1-25. <https://doi.org/10.1007/s11220-021-00336-4>.
- Reddy, J.N. (2006), *Theory and Analysis of Elastic Plates and Shells (2nd ed.)*, CRC Press, Florida, U.S.A.
- Reddy, J.N. (2007), "Nonlocal theories for bending, buckling and vibration of beams", *Int. J. Eng. Sci.*, **45**(2-8), 288-307. <https://doi.org/10.1016/j.ijengsci.2007.04.004>.
- Reddy, J.N. (2010), "Nonlocal nonlinear formulations for bending of classical and shear deformation theories of beams and plates", *Int. J. Eng. Sci.*, **48**(11), 1507-1518. <https://doi.org/10.1016/j.ijengsci.2010.09.020>.
- Shi, W., Guo, Y., Zhang, Z. and Guo, W. (2019), "Strain gradient mediated magnetism and polarization in monolayer V Se₂", *J. Phys. Chem. C*, **123**(40), 24988-24993. <https://doi.org/10.1021/acs.jpcc.9b08445>.
- Shi, Y., Li, N., Ye, J. and Ma, J. (2021), "Enhanced magneto-electric response in nanostructures due to flexoelectric and flexomagnetic effects", *J. Magn. Magn. Mater.*, **521**, 167523. <https://doi.org/10.1016/j.jmmm.2020.167523>.
- Shingare, K.B. and Kundalwal, S.I. (2019), "Static and dynamic response of graphene nanocomposite plates with flexoelectric effect", *Mech. Mater.*, **134**, 69-84. <https://doi.org/10.1016/j.mechmat.2019.04.006>.
- Sidhardh, S. and Ray, M.C. (2018), "Flexomagnetic response of nanostructures", *J. Appl. Phys.*, **124**(24), 244101. <https://doi.org/10.1063/1.5060672>.
- Sladek, J., Sladek, V., Xu, M. and Deng, Q. (2021), "A cantilever beam analysis with flexomagnetic effect", *Meccanica*, **56**(9), 2281-2292. <https://doi.org/10.1007/s11012-021-01357-9>.
- Sun, X.P., Hong, Y.Z., Dai, H.L. and Wang, L. (2017), "Nonlinear frequency analysis of buckled nanobeams in the presence of

longitudinal magnetic field”, *Acta Mechanica Solida Sinica*, **30**(5), 465-473. <https://doi.org/10.1016/j.camss.2017.08.002>.

Wang, B. and Li, X.F. (2021), “Flexoelectric effects on the natural frequencies for free vibration of piezoelectric nanoplates”, *J. Appl. Phys.*, **129**(3), 034102. <https://doi.org/10.1063/5.0032343>.

Xu, X. and Zheng, M. (2019), “Analytical solutions for buckling of size-dependent Timoshenko beams”, *Appl. Math. Mech.*, **40**(7), 953-976. <https://doi.org/10.1007/s10483-019-2494-8>.

Zhang, J.X., Zeches, R.J., He, Q., Chu, Y.H. and Ramesh, R. (2012), “Nanoscale phase boundaries: A new twist to novel functionalities”, *Nanoscale*, **4**(20), 6196-6204. <http://doi.org/10.1039/C2NR31174G>.

Zhang, N., Zheng, S. and Chen, D. (2019), “Size-dependent static bending of flexomagnetic nanobeams”, *J. Appl. Phys.*, **126**(22), 223901. <https://doi.org/10.1063/1.5128940>.

JL

Appendix

The plane-stress reduced stiffnesses and extensional and bending stiffness coefficients appearing in Eqs. (15), and (32)-(35) are defined as:

$$Q_{11} = \frac{E}{1 - \nu^2}, \quad Q_{12} = \frac{E\nu}{1 - \nu^2} \quad (A1)$$

$$\begin{aligned} A_{11} &= \int_{-h/2}^{h/2} Q_{11} dz = Q_{11}h, \\ A_{55} &= \int_{-h/2}^{h/2} C_{55} dz = C_{55}h, \end{aligned} \quad (A2)$$

$$D_{11} = \int_{-h/2}^{h/2} Q_{11} z^2 dz = \frac{Q_{11}h^3}{12}$$

Also, the coefficients appearing in Eqs. (56) and (57) for the DFM effect are defined as:

$$P_1 = K_s A_{55} (I_{20} - l^2 I_{40}) + N_{xx}^T (-I_{20} + \mu I_{40})$$

$$M_1 = K_s A_{55} \left(l^2 \int_0^a \frac{d^4 h}{dx^4} N_i dx - \int_0^a \frac{d^2 h}{dx^2} N_i dx \right)$$

$$N_1 = K_s A_{55} \left(\int_0^a \frac{d\theta_i}{dx} N_i dx - l^2 \int_0^a \frac{d^3 \theta_i}{dx^3} N_i dx \right)$$

$$K_1 = \frac{A_{11} a_{33} + h d_{31}^2}{a_{33}} \frac{1}{2a} I_{11} (I_{20} - \mu I_{40}) \quad (A3)$$

$$G_1 = \frac{A_{11} a_{33} + h d_{31}^2}{a_{33}} \frac{1}{2a} (\mu I_{40} - I_{20}) \int_0^a \left(\frac{dh}{dx} \right)^2 dx$$

$$P_2 = K_s A_{55} \left(l^2 \int_0^a \frac{d^3 N_i}{dx^3} \theta_i dx - \int_0^a \frac{dN_i}{dx} \theta_i dx \right)$$

$$M_2 = K_s A_{55} \left(\int_0^a \frac{dh}{dx} \theta_i dx - l^2 \int_0^a \frac{d^3 h}{dx^3} \theta_i dx \right)$$

$$N_2 = \bar{D} (J_{20} - l^2 J_{40}) + K_s A_{55} (l^2 J_{20} - J_{00})$$

and, for the CFM effect these coefficients are defined as:

$$P_1 = K_s A_{55} (I_{20} - l^2 I_{40}) + (N_{xx}^T - d_{31} \Psi_1) (-I_{20} + \mu I_{40})$$

$$M_1 = K_s A_{55} \left(l^2 \int_0^a \frac{d^4 h}{dx^4} N_i dx - \int_0^a \frac{d^2 h}{dx^2} N_i dx \right)$$

$$N_1 = K_s A_{55} \left(\int_0^a \frac{d\theta_i}{dx} N_i dx - l^2 \int_0^a \frac{d^3 \theta_i}{dx^3} N_i dx \right)$$

$$K_1 = \frac{A_{11}}{2a} I_{11} (I_{20} - \mu I_{40}) \quad (A4)$$

$$G_1 = \frac{A_{11}}{2a} (\mu I_{40} - I_{20}) \int_0^a \left(\frac{dh}{dx} \right)^2 dx$$

$$P_2 = K_s A_{55} \left(l^2 \int_0^a \frac{d^3 N_i}{dx^3} \theta_i dx - \int_0^a \frac{dN_i}{dx} \theta_i dx \right)$$

$$M_2 = K_s A_{55} \left(\int_0^a \frac{dh}{dx} \theta_i dx - l^2 \int_0^a \frac{d^3 h}{dx^3} \theta_i dx \right)$$

$$N_2 = \bar{D} (J_{20} - l^2 J_{40}) + K_s A_{55} (l^2 J_{20} - J_{00})$$

where

$$\begin{aligned} I_{20} &= \int_0^a \frac{d^2 N_i}{dx^2} N_i dx, \quad I_{40} = \int_0^a \frac{d^4 N_i}{dx^4} N_i dx, \quad I_{11} = \int_0^a \frac{dN_i}{dx} \frac{dN_i}{dx} dx, \\ J_{20} &= \int_0^a \frac{d^2 \theta_i}{dx^2} \theta_i dx, \quad J_{40} = \int_0^a \frac{d^4 \theta_i}{dx^4} \theta_i dx, \quad J_{00} = \int_0^a \theta_i \theta_i dx \end{aligned} \quad (A5)$$